UNIVERSIDAD DISTRITAL
FRANCISCO JOSÉ DE CALDAS

Revista Científica

http://revistas.udistrital.edu.co/ojs/index.php/revcie/index

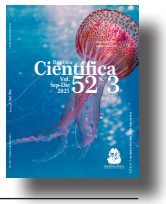

Artículo de investigación científica

New Lithium Bis(trifluoromethanesulfonyl)imide Electrolytes Based on Rice Starch

Nuevos electrolitos de bis(trifluorometanosulfonil)imida de litio basados en almidón de arroz

Novos eletrólitos de bis(trifluorometanossulfonil)imida de lítio baseados em amido de arroz

Miguel Iban Delgado Rosero[1]
Nori Magali Jurado Meneses[2]
Ramiro Uribe Kaffure[3]

Recibido: 18 de julio de 2025 **Aceptado:** 21 de diciembre de 2025

Para citar este artículo: Delgado, M. I., Jurado, N. M., y Uribe, R. (2025). New Lithium Bis(trifluoromethanesulfonyl) imide Electrolytes Based on Rice Starch. *Revista Científica*, *52*(3), 25-39. https://doi.org/10.14483/23448350.23926

Abstract

In this work, biopolymer electrolyte membranes based on rice starch and $CF_3SO_2NLiSO_2CF_3$ (LiTFSI) were prepared via the solution casting method and characterized by impedance spectroscopy (IS), differential scanning calorimetry (DSC), and cyclic voltammetry (CV). The graphs of the ionic conductivity logarithm as a function of the inverse of the temperature exhibit an Arrhenius behavior, which indicates a thermally activated conduction process, while the DSC results reveal a step-shaped anomaly associated with the glass transition temperature (Tg) of a new polymer complex. The cyclic voltammetry analysis suggests a qualitative electrochemical stability range between -2.5 and +2.5 V. At room temperature, the highest ionic conductivity obtained was higher than 9×10^{-3} $S{\cdot}cm^{-1}$ for the membrane containing 50 wt.% LiTFSI. Despite the notable enhancement in ionic conductivity, membranes with higher salt content exhibit reduced mechanical robustness and may be affected by residual moisture. These findings highlight the potential of rice starch-LiTFSI systems as promising candidates for future electrochemical devices, although further optimizations are required, such as mechanical reinforcement and more detailed stability assessments for practical implementation.

Keywords: polymer electrolytes, ionic conductivity, biopolymers, starch, impedance spectroscopy

1. Departamento de Física, Universidad del Tolima, Colombia. Contacto: mirosero@ut.edu.co
2. Departamento de Física, Universidad del Tolima, Colombia. Contacto: nmjuradom@ut.edu.co
3. Departamento de Física, Universidad del Tolima, Colombia. Contacto: rauribe@ut.edu.co

Resumen

En este trabajo se prepararon membranas de electrolito biopolimérico a base de almidón de arroz y $CF_3SO_2NLiSO_2CF_3$ (LiTFSI) mediante el método de solución y se caracterizaron mediante espectroscopía de impedancia (IS), calorimetría diferencial de barrido (DSC) y voltametría cíclica (CV). Las gráficas del logaritmo de la conductividad iónica en función del inverso de la temperatura se ajustan a un modelo de tipo Arrhenius, lo que indica un proceso de conducción térmicamente activado, mientras los resultados de DSC revelaron una anomalía en forma de escalón asociada a la temperatura de transición vítrea (Tg) de un nuevo complejo polimérico. El análisis de voltametría cíclica sugiere un rango cualitativo de estabilidad electroquímica entre -2.5 V y +2.5 V. A temperatura ambiente, la mayor conductividad iónica obtenida fue superior a 9×10^{-3} S·cm^{-1} para la membrana con 50 wt.% LiTFSI. A pesar del notable incremento en la conductividad iónica, las membranas con mayor contenido de sal presentan una menor robustez mecánica y pueden verse afectadas por la humedad residual. Estos resultados destacan el potencial de los sistemas almidón de arroz-LiTFSI como candidatos prometedores para futuros dispositivos electroquímicos, si bien se requieren optimizaciones adicionales, como el refuerzo mecánico y evaluaciones más detalladas de estabilidad para su implementación práctica.

Palabras clave: electrolitos poliméricos, conductividad iónica, biopolímeros, almidón, impedancia, espectroscopía

Resumo

Neste trabalho prepararam-se membranas de eletrólito biopolimérico baseado em amido de arroz e $CF_3SO_2NLiSO_2CF_3$ (LiTFSI) através do método de solução e caracterizaram-se por meio de espectroscopia de impedância (IS), calorimetria diferencial de barrido (DSC) e voltametria cíclica (CV). Os gráficos do logaritmo da condutividade iónica em função do inverso da temperatura ajustam-se a um modelo de tipo Arrhenius, o que indica um processo de condução termicamente ativado, enquanto os resultados de DSC revelaram uma anomalia em forma de degrau associada à temperatura de transição vítrea (Tg) de um novo complexo polimérico. A análise de voltametria cíclica sugere uma faixa qualitativa de estabilidade eletroquímica entre -2.5 e + 2.5 V. À temperatura ambiente, a maior condutividade iônica obtida foi superior a 9×10^{-3} S·cm^{-1} para a membrana com 50% em peso de LiTFSI. Apesar do notável aumento na condutividade iônica, as membranas com maior conteúdo de sal apresentam menor robustez mecânica e podem ser afetadas pela umidade residual. Esses resultados destacam o potencial dos sistemas amido de arroz-LiTFSI como candidatos promissórios para futuros dispositivos eletroquímicos, ainda se requeiram otimizações adicionais, como reforçamento mecânico e avaliações de estabilidade mais detalhadas para sua implementação prática.

Palavras-chaves: eletrólitos poliméricos, condutividade iônica, biopolímeros, amido, impedância, espectroscopia

INTRODUCTION

The development of biopolymer-based electrolytes has attracted considerable attention due to their sustainability, low cost, and compatibility with flexible electrochemical devices (Sharma & Banerjee, 2025). Notably, starch-based polymer solid electrolytes have emerged as a promising alternative to synthetic polymer-based electrolytes, given their natural abundance and high biodegradability (Yadav *et al.*, 2023).

Research on solid polymer electrolytes based on starch and other naturally derived polymers constitutes a field of great interest due to the advantages they offer in terms of environmental sustainability and performance. The widespread availability of such materials, coupled with the ongoing enhancement of their properties, render them an attractive option for the battery industry and other energy storage device applications.

The incorporation of natural polymers, such as starch, cellulose, chitin, and lignin, has facilitated improvements in the properties of solid polymer electrolytes (Aziz *et al.*, 2024; Hina *et al.*, 2024; Yang *et al.*, 2024). The structural composition of starch comprises two glucose polymers: linear amylose and highly branched amylopectin. Amylose molecules typically comprise 200-20 000 glucose units arranged in a helical conformation, as a consequence of the bond angles established between the glucose units. Conversely, amylopectin exhibits short lateral glucose branches linked to a main chain composed of 20 to 30 glucose units. The hydroxyl groups in the amylose and amylopectin chains can coordinate with Li^+ ions, providing ionic transport pathways. Recent structural studies indicate that the starch present in most species contains water within its molecular structure, which facilitates conduction by promoting ion dissociation (Chatterjee *et al.*, 2016; Tang & Alavi, 2011).

On the other hand, lithium bis-trifluoromethanesulfonimide salt (LiTFSI) has been used as an electrolyte in high-temperature lithium batteries, replacing lithium hexafluorophosphate ($LiPF_6$) (Kalhoff *et al.*, 2014). This salt has also been used in the synthesis of solid polymer electrolytes, in combination with polyethylene oxide (PEO), polymethyl methacrylate (PMMA), and polyvinyl alcohol (PVA) (Dennis *et al.*, 2023; Gucci *et al.*, 2023; Jagan & Vijayachamundeeswari, 2023), showing high conductivity values and suitable mechanical, thermal, and electrochemical properties. It exhibits high ionic dissociation due to the large and highly delocalized nature of its $TFSI^-$ anion, which minimizes electrostatic interactions with Li^+ and promotes complete salt dissociation. This leads to a higher concentration of mobile lithium ions, enhancing ionic conductivity in polymer-based electrolytes. Additionally, LiTFSI offers superior thermal and electrochemical stability compared to $LiPF_6$, particularly under elevated temperatures, making it a suitable choice for solid-state lithium batteries and other high-temperature electrochemical applications involving electrochemical devices (Yue *et al.*, 2025).

Solid polymer electrolytes synthesized from natural components have attracted increasing attention due to their accessibility, biodegradability, biocompatibility, and low reactivity with solid lithium, making them promising candidates for energy storage applications. Previous studies have investigated systems based on corn starch (Yadav *et al.*, 2023), potato starch (Rai *et al.*, 2025), and other biopolymers (Arrieta *et al.*, 2023; Aziz *et al.*, 2024), including approaches involving cross-linked starch and nanocomposite formulations, reporting ionic conductivities typically in the order of 10^{-3} $S{\cdot}cm^{-1}$ under similar conditions (Arrieta *et al.*, 2024). However, the specific combination of rice starch (a high-amylose, film-forming polysaccharide) with LiTFSI remains underexplored, despite its potential to enhance ion mobility and amorphization within the polymer matrix.

Rice starch was selected since its relatively high amylose content promotes stronger intermolecular interactions and enables the formation of uniform, self-supporting films. Furthermore, since this research was conducted in a region with extensive rice cultivation, the use of rice starch enables the valorization of a locally abundant resource, supporting sustainable development and cost-effective material production. These advantages make rice starch a strategic and promising alternative to other natural polymers.

In this vein, this study focused on the preparation and electrical and thermal characterization of solid polymer electrolytes based on rice starch and LiTFSI salt, which would offer the advantage of a highly mobile cation within the polymer matrix. Future works will include FTIR, XRD, and SEM/AFM analyses to complement the findings presented herein.

EXPERIMENTAL DETAILS

Membrane preparation

Aqueous solutions were prepared and poured onto glass Petri dishes for drying in a low humidity environment not exceeding 30% relative humidity (this was achieved by incorporating silica gel inside the desiccator). After the drying process, membranes with a diameter of 10 cm (0.10 m) and a thickness ranging from 0.70 to 0.90 mm ($7.0x10^{-3}$ to $9.0x10^{-3}$ m) were obtained.

Starch-LiTFSI combinations were prepared at mass percentages of 35, 40, 50, 60, and 70%, which were calculated according to the following Equation:

$$wt = \frac{m_{salt}}{m_{salt} + m_{polimer}} * 100 \quad (1)$$

The starch quantities were determined using an analytical balance (0.1 mg precision) and dissolved in water at a 3.0% w/v concentration via magnetic stirring at 363 K for two hours. Similarly, the LiTFSI masses, measured with 0.1 mg ($1x10^{-6}$ kg) precision, were dissolved in water at a 3.0% w/v concentration through magnetic stirring at room temperature for 30 min. Once the starch had been completely dissolved, a viscous semi-transparent liquid was obtained. This liquid was slowly cooled to room temperature, after which the two solutions were combined and stirred for an additional two hours.

The resulting liquid was deposited into glass Petri dishes and placed in a desiccator with silica gel to maintain low humidity and room temperature, allowing for solvent evaporation. After four days, semi-transparent membranes such as those shown in Figure 1 were obtained and kept at low humidity (below 40%) until experimental analysis was performed.

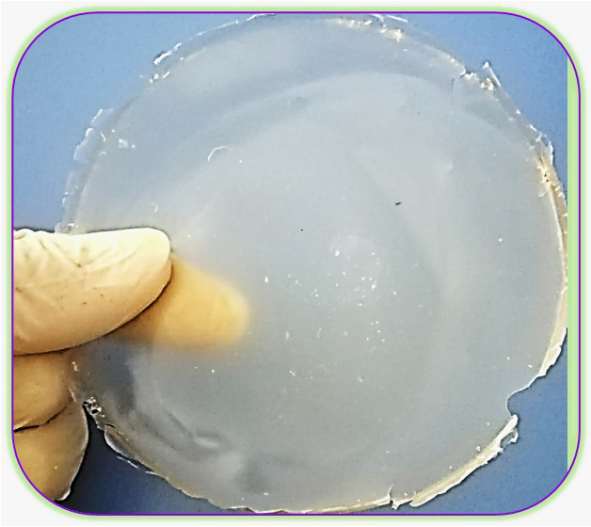

Figure 1. *Starch-LiTFSI membrane at a concentration of 40.0 wt.%*

Although starch-based systems often require a chemical crosslinker to form stable films, in this work, rice starch-LiTFSI membranes were successfully obtained without any crosslinking agent. This can be attributed to the high amylose content of rice starch, which promotes gelatinization and network formation through intermolecular hydrogen bonding during drying (Mali *et al.*, 2010).

Sample characterization

Sample characterization included impedance spectroscopy (IS) analysis, differential scanning calorimetry (DSC), and cyclic voltammetry (CV).

IS involves applying an alternating voltage to a sample in order to determine its real and imaginary impedance values by measuring the current flow at different temperatures. The set of impedance and frequency values obtained is known as the *impedance spectrum*.

For IS measurements, membrane discs with a 7 mm ($7x10^{-3}$ m) diameter were cut and placed between two stainless steel electrodes in a sandwich configuration. An alternating potential of 0.4 V was applied using a Hioki 3532 impedance analyser over a frequency range of 50 Hz to 5 MHz. The temperature of this impedance measurement cell was controlled by a furnace. Measurements were taken at constant temperature every 5 K. An AC amplitude of 0.4 V was selected to ensure an adequate signal-to-noise ratio for this solid electrolyte system. Note that this value is well below the electrochemical stability window determined by CV (-2.5 to +2.5 V), ensuring that no faradaic reactions or material degradation occur during the measurements. Additionally, the impedance spectra for this—and for other polymer electrolytes (Zougar *et al.*, 2008)—showed no dependence on the applied amplitude, confirming that the system operated within a linear and non-faradaic response regime. We employed CV at a scan rate of 10 mV s^{-1} to quantitatively determine the electrochemical stability window (Méry *et al.*, 2021) with a symmetrical SS/electrolyte/SS cell (SS: stainless steel). The same electrode area was used for all samples. This configuration has been previously reported by D. Kumar and K. Mishra (Kumar & Hashmi, 2010; Mishra *et al.*, 2017).

DSC characterization allows studying the heat flow as a function of temperature. In this work, DSC measurements were conducted using a DSC 131 Evo calorimeter. This equipment allows for measurements in the temperature range between 103 and 973 K. This range is suitable for studying the thermal properties of

materials like polymers, as well as for analyzing thermal variations such as the glass transition temperature (T_g) and the melting temperature (T_m).

RESULTS AND DISCUSSION

It should be clarified that, considering the effect of residual moisture on the conductivity values, special care was taken to minimize the influence of water on impedance measurements. To remove superficial moisture from the membranes, the samples were conditioned at a relative humidity of approximately 10% and at room temperature for 24 hours prior to the impedance analysis. This controlled drying procedure ensured reproducible and reliable electrochemical results, reducing the contribution of absorbed water to the overall ionic conductivity.

In Figure 2a, impedance spectra are presented as Nyquist plots, showing the imaginary impedance (Z'') as a function of the real impedance (Z') for a starch-LiTFSI membrane at a 40 wt.% salt concentration. The plots exhibit a depressed semicircle at high frequencies, followed by an inclined line at low frequencies. The linear region corresponds to the capacitive behavior at the electrode-electrolyte interface, while the shape and size of the

semicircle provide information about the electrical properties of the material. As temperature increases, the semicircle diameter decreases, indicating a reduction in bulk resistance due to thermally activated ion mobility. This behavior is characteristic of ion-conducting polymer electrolytes, and it is consistent with the correlated barrier hopping (CBH) mechanism reported for amorphous ionic conductors (Yong, Chen, *et al.*, 2025; Yong, Winie, *et al.*, 2025). The inset in Figure 2a shows an enlarged view of the Nyquist plot at room temperature for the 40 wt.% concentration, together with its corresponding fit to the equivalent circuit model.

Figure 2b shows a Nyquist plot for the membrane with the highest ionic conductivity (50 wt.% LiTFSI). This plot incorporates the equivalent circuit, composed of a bulk resistance R_1 in parallel with a constant phase element (CPE_1), in series with two additional CPE components (CPE_0 and CPE_2). The circuit fitting was performed at room temperature (298 K), enabling an accurate extraction of R_1. The high-frequency intercept of the fitted curve confirms the absence of short-circuit artifacts and excessive electrode polarization, supporting the intrinsic nature of the high ionic conductivity reported for this concentration.

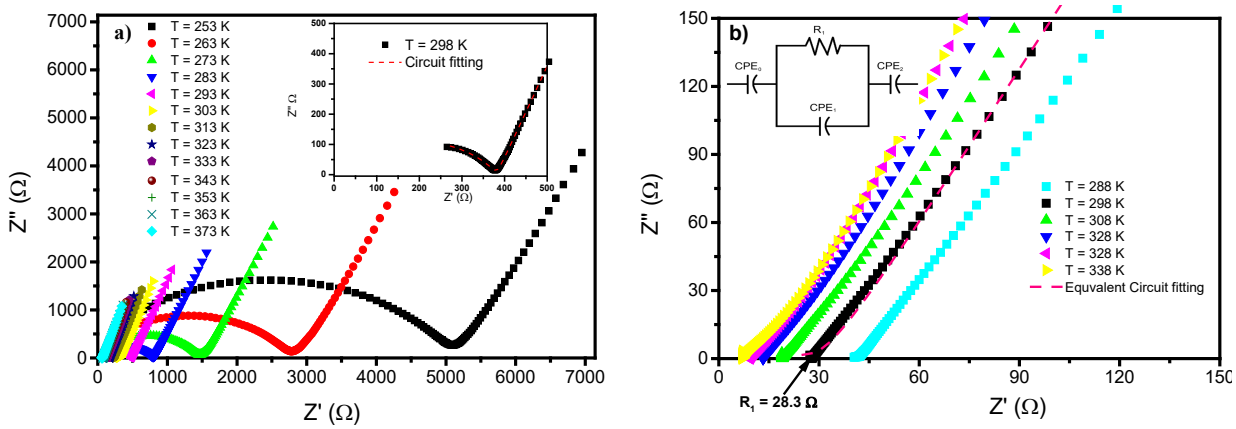

Figure 2. *Nyquist plots for a starch-LiTFSI membrane at different temperatures: a) concentration of x = 40 wt.%, b) concentration of x = 50 wt.%*

The fitting parameters obtained from the equivalent circuit (including R_1 and CPE elements) are presented in Table 1, showing good agreement between the model and the experimental data.

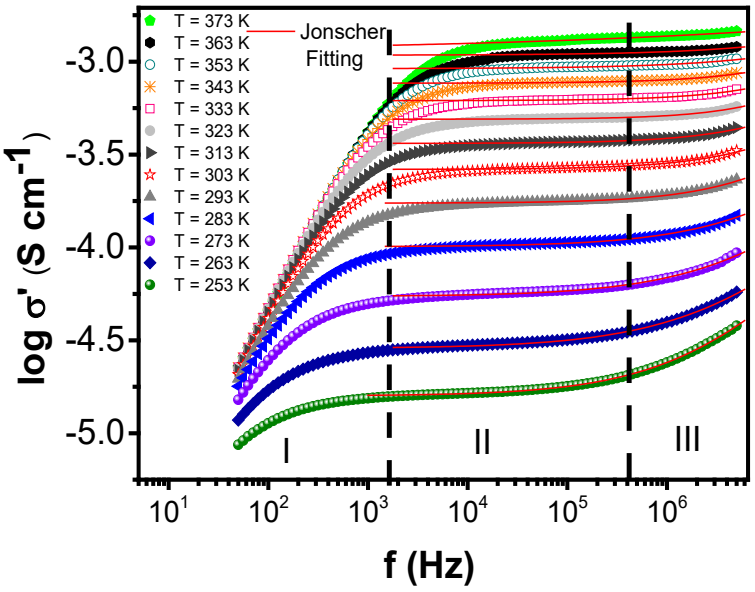

Figure 3. *Logarithm of the real conductivity as a function of the logarithm of frequency for a starch-LiTFSI electrolyte concentration of 40.0 wt.%*

Table 1. *Fitting parameters for the equivalent circuit, obtained from Nyquist plots of starch-LiTFSI polymer electrolytes at 298 K*

Concentration (% wt)	R_1 (Ω)	CPE_0		CPE_1		CPE_2	
		C_0 (F)	θ_0	C_1 (F)	θ_1	C_2 (F)	$_2$
40	382.33	5.64×10^{-06}	7.98×10^{-1}	1.34×10^{-8}	6.65×10^{-1}	3.73×10^{2}	2.91×10^{-1}
50	25.54	2.38×10^{-06}	7.41×10^{-1}	2.54×10^{-4}	1	2.01×10^{-2}	3.94×10^{-2}

Figure 3 shows logarithmic plots of real conductivity (σ') as a function of the logarithm of frequency (f) (Bode plots). These diagrams exhibit three distinct regions: region I, at low frequencies, where conductivity increases rapidly with frequency due to interfacial polarization phenomena caused by double-layer effects at blocking electrodes; region II, where real conductivity remains constant over a wide frequency range, allowing for the calculation of direct-current conductivity (σ_{dc}); and region III, at high frequencies, where a characteristic dispersion attributed to the hooping mechanism is observed—associated with short-range ionic migration (Arya & Sharma, 2019).

As shown in Figure 3, the data in regions II and III fit the Jonscher equation (solid red lines):

$$\sigma'(\omega) = \sigma_{dc}\left[1 + \left(\frac{\omega}{\omega_p}\right)^n\right] \quad (2)$$

where σ_{dc} is the direct-current (DC) conductivity of the sample, ω is the angular frequency ($\omega = 2\pi f$), ω_p is the characteristic frequency at which the transition from constant to dispersive behavior occurs, and *n* is the exponent associated with the conduction mechanism.

The exponent *n* was observed to decrease with increasing temperature, indicating that the hopping process becomes more correlated as temperature rises. This behavior supports the CBH model, where ions hop over potential barriers separating localized sites. At higher temperatures, thermal energy reduces the effective barrier height, facilitating long-range ion transport. Therefore, the conduction mechanism in the rice starch-LiTFSI electrolyte can be primarily attributed to CBH, consistent with similar biopolymer systems (Yong, Chen, *et al.*, 2025).

Table 2 lists the parameter values obtained from fitting the Jonscher equation to the x = 40% sample. As the temperature increases, the DC conductivity in region II also increases, a characteristic feature of thermally activated ionic motion. This behavior is commonly observed in solid polymer electrolytes composed of polymers and alkali salts (Jurado *et al.*, 2013). Furthermore, note that the values of the power law exponent *n* fall within the range of 0 to 1, as typically observed in such systems (P. Singh *et al.*, 2019).

Table 2. *Parameters from the Jonscher fit for a concentration of x = 40 wt.% different temperatures.*

T (K)	σ_{dc} (S cm^{-1})	B (S cm^{-1})Hz	n ± 0.005
253.0	$1.60 \times 10^{-5} \pm 1.06 \times 10^{-8}$	$3.01 \times 10^{6} \pm 7.79 \times 10^{3}$	0.6136
263.0	$2.94 \times 10^{-5} \pm 3.21 \times 10^{-8}$	$5.49 \times 10^{6} \pm 2.43 \times 10^{4}$	0.5670
273.0	$5.64 \times 10^{-5} \pm 1.21 \times 10^{-7}$	$9.76 \times 10^{6} \pm 1.35 \times 10^{5}$	0.5731
283.0	$1.03 \times 10^{-4} \pm 1.89 \times 10^{-7}$	$1.69 \times 10^{7} \pm 4.61 \times 10^{5}$	0.5960
293.0	$1.03 \times 10^{-4} \pm 1.92 \times 10^{-7}$	$1.70 \times 10^{7} \pm 4.85 \times 10^{5}$	0.6920
303.0	$1.75 \times 10^{-4} \pm 3.06 \times 10^{-7}$	$2.39 \times 10^{7} \pm 9.89 \times 10^{5}$	0.6786
313.0	$2.66 \times 10^{-4} \pm 4.82 \times 10^{-7}$	$3.11 \times 10^{7} \pm 1.99 \times 10^{6}$	0.6796
323.0	$3.67 \times 10^{-4} \pm 6.49 \times 10^{-7}$	$3.86 \times 10^{7} \pm 3.30 \times 10^{6}$	0.7592
333.0	$4.95 \times 10^{-4} \pm 6.34 \times 10^{-7}$	$3.84 \times 10^{7} \pm 3.06 \times 10^{6}$	0.6902
343.0	$6.26 \times 10^{-4} \pm 9.24 \times 10^{-7}$	$4.18 \times 10^{7} \pm 4.35 \times 10^{6}$	0.6568
353.0	$7.80 \times 10^{-4} \pm 9.60 \times 10^{-7}$	$4.03 \times 10^{7} \pm 3.66 \times 10^{6}$	0.4964
363.0	$9.36 \times 10^{-4} \pm 1.67 \times 10^{-6}$	$7.87 \times 10^{7} \pm 1.37 \times 10^{7}$	0.4961
373.0	$0.0011 \pm 1.94 \times 10^{-6}$	$1.12 \times 10^{8} \pm 2.12 \times 10^{7}$	0.1484

In Figure 4, plots of the logarithm of DC conductivity as a function of the inverse of temperature are shown for starch-LiTFSI membranes at different concentrations. These graphs illustrate a significant increase in conductivity with rising temperature, following an Arrhenius-like behavior in accordance with Equation (3).

$$\sigma_{dc} = \sigma_0 exp^{\left(-\frac{E_A}{K_B T}\right)} \quad (3)$$

where σ_0 is a pre-exponential factor, E_A is the activation energy, k_B is the Boltzmann constant, and T is the absolute temperature.

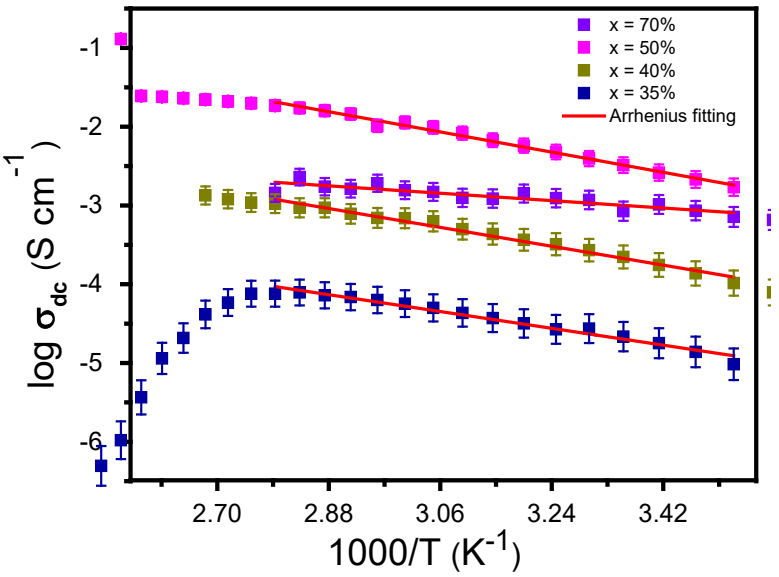

Figure 4. *Plots of the logarithm of conductivity as a function of the inverse of temperature for different concentrations of starch-LiTFSI electrolytes*

The increase in conductivity with rising temperature (observed in all plots in Figure 4)_which is characteristic of semicrystalline solid polymer electrolytes—indicates that the ionic conduction process in this system is thermally activated (Bandara *et al.*, 2020). An anomalous behavior was noted for the x = 35% concentration, which exhibits a sharp decline in conductivity at 370 K, attributed to the evaporation of residual solvents from sample preparation or to moisture absorbed by the membrane.

The Arrhenius fitting parameters for the plots depicted in Figure 4 are detailed in Table 3. This table includes the values of the logarithm of conductivity at maximum temperature (log σ_0) and the activation energy, representing the energy required for an ion to transition to another coordination site. The activation energy values, ranging from 0.20 to 0.28 eV, are comparable to those typically reported for lithium-salt-based biopolymer electrolytes (Bradford *et al.*, 2022; Dennis *et al.*, 2023; Jansi *et al.*, 2023), confirming that the ionic transport mechanism falls within the expected range for these systems

Table 3. *Parameters from the Arrhenius fit in plots of log conductivity vs. 1000/T for starch-LiTFSI electrolyte samples*

x (wt.%)	Log σ_0 (S.cm^{-1})	E_A ±0.01 (eV)
35	5.6x10^{-4}	0.24
40	8.9x10^{-4}	0.27
50	1.1x10^{-3}	0.28
70	2.4x10^{-3}	0.20

The logarithm of DC conductivity as a function of the system's LiTFSI concentration is depicted in Figure 5. It is evident that, with an increase in the LiTFSI concentration, the conductivity also increases, a phenomenon attributed to the rise in the number of charge carriers within the polymer matrix. At room temperature (298 K), the maximum conductivity value of 9.79 x 10^{-3} S cm^{-1} was achieved at a concentration of x = 50%. Notably, for the highest concentration analyzed (x = 70%), a decrease in conductivity with respect to x = 50% was observed, likely due to the ionic association that blocks the conduction pathways (Mart, 2017; C. P. Singh *et al.*, 2020).

To put our results into context, the ionic conductivity of the rice starch-LiTFSI system was compared against previously reported starch-based and biopolymer nanocomposite electrolytes. For instance, cross-linked starch electrolytes have shown conductivities of 2.7 x 10^{-3} S·cm^{-1} (Arrieta *et al.*, 2024), while biopolymer nanocomposites have reached between 1.12 x 10^{-5} and 3.32 x 10^{-2} S·cm^{-1} (Bósquez-Cáceres *et al.*, 2021; Ong *et al.*, n.d.).

Although ionic conductivity increases with a higher LiTFSI content, this improvement is accompanied by a reduction in the mechanical stability of the membranes. The greater number of ionic species disrupts the polymer chain packing, resulting in a more plasticized and less cohesive structure that becomes fragile at high salt concentrations. Therefore, the best electrochemical performance does not necessarily translate into suitable handling properties for practical applications. Future improvements may rely on reinforcement strategies, such as polymer blending with mechanically stronger biopolymers or the incorporation of plasticizers/binders like glycerol or sorbitol to enhance flexibility and cohesion without significantly affecting the ionic transport.

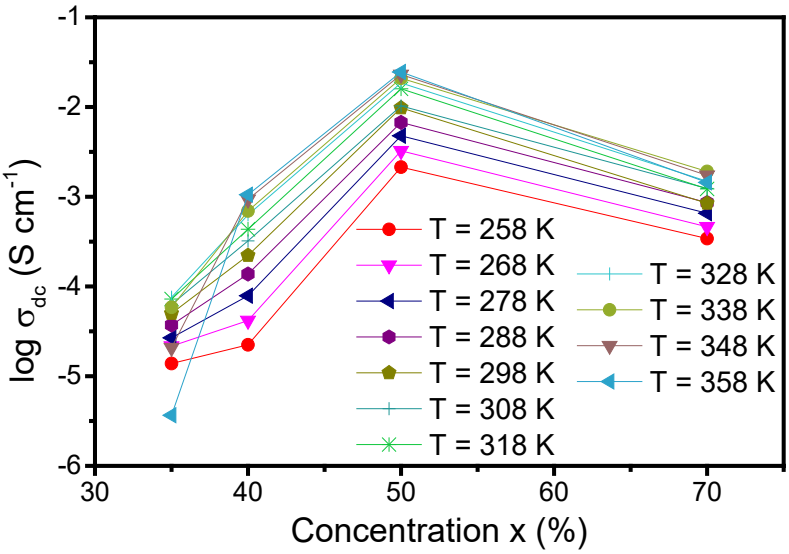

Figure 5. *Logarithm of conductivity as a function of concentration for different temperatures of starch-LiTFSI membranes*

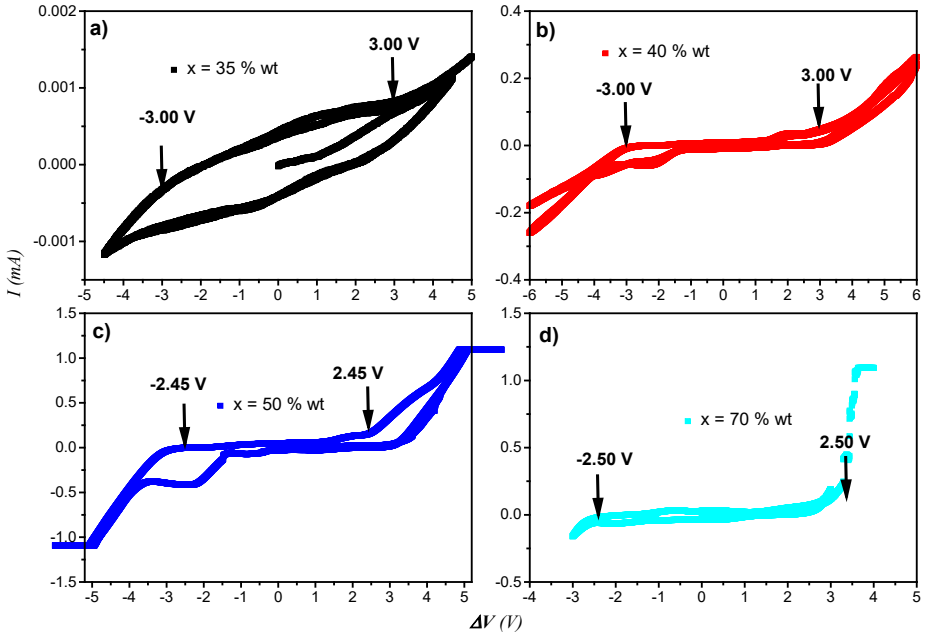

Figure 6. *CV measurements for starch-LiTFSI polymer electrolytes: a) x = 35 wt.%, b) x = 40 wt.%, c) x = 50 wt.%, d) x = 70 wt.%*

The cyclic voltammogram curves for starch-LiTFSI electrolytes are presented in Figure 6. The electrochemical stability window is -3.00 to 3.00 V for x = 35 and 40 wt.%, whereas, for x = 50 and 70 wt.%, it narrows to -2.45 to 2.45 V.

The electrochemical stability window of the starch-LiTFSI polymer electrolytes was evaluated via CV using stainless steel electrodes at room temperature. Measurements performed at a scan rate of 10 $mV \cdot s^{-1}$ revealed negligible current flow across the applied potential range. No significant faradaic redox peaks or irreversible decomposition features were detected within approximately -2.5 to +2.5 V, suggesting that the response is dominated by capacitive behavior at the electrode-electrolyte interface.

Figure 7 shows the DSC thermograms for LiTFSI salt, rice starch, and polymeric membranes with different LiTFSI concentrations. The thermogram corresponding to LiTFSI salt exhibits an endothermic peak at 317 K, which has been attributed to the salt's melting point. The thermogram of a rice starch membrane displays a broad endothermic peak around 353 K, associated with the melting of this polymer's crystalline phase. This anomaly can also be observed in the synthesized membranes combining starch and LiTFSI at concentrations of x = 30, 35, and 50%. However, this peak is absent at higher concentrations, leading to the conclusion that the crystalline phase of rice starch disappears when combined with high salt concentrations.

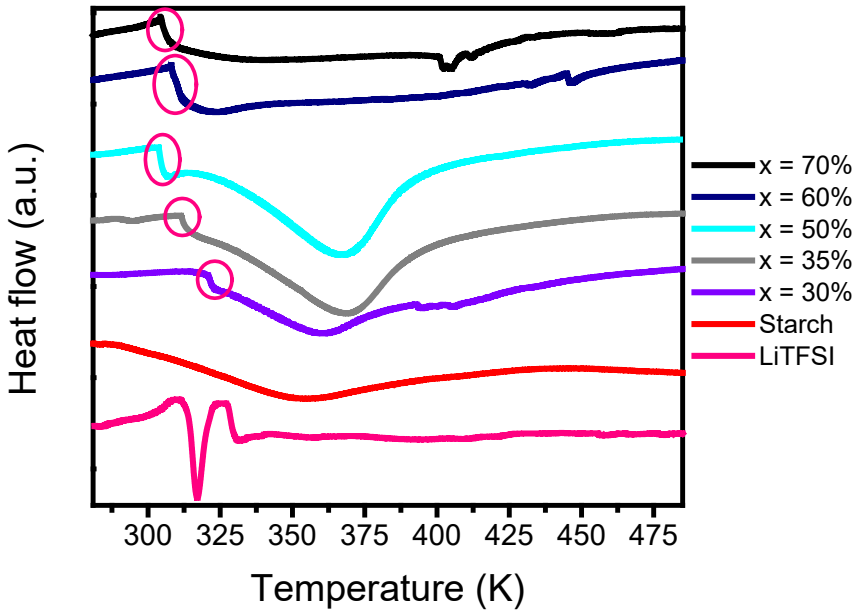

Figure 7· *DSC thermograms for LiTFSI salt, rice starch, and different concentrations of starch-LiTFSI electrolytes*

In the thermograms of the membranes formed by combinations of starch and LiTFSI salt, a step-like anomaly is observed at 321 K. This is associated with the system T_g. The temperature at which this anomaly occurs slightly decreases as the salt concentration increases, indicating an increase in the fraction of the amorphous phase in the system. This phenomenon could explain the increase in conductivity observed in the impedance measurements, as the amorphous phase promotes ionic mobility and salt dissociation (Rasali *et al.*, 2019; Whba *et al.*, 2020).

Table 4 presents the glass transition temperatures obtained at the midpoint of the heat flow change region. Note that the values for membranes with high concentrations of LiTFSI salt are lower, indicating a higher degree of amorphicity in these membranes. Furthermore, the endothermic peak representing the melting of the starch crystalline phase shows variations in enthalpy values, indicating changes in the crystalline phase. The enthalpy values obtained by integrating the curve in the region of the endothermic peak are also shown in this Table.

Table 4. *Glass transition temperatures for starch-LiTFSI electrolytes*

x wt.%)	T_g (K)	T_m (K)	ΔH (J g^{-1})
LiTFSI	309.8	317.1	17.323
Starch	284.6	351.1	59.240
30	315.8	361.2	55.303
35	311.4	369.5	183.421
50	302.5	367.2	204.839
60	308.1	318.9	3.178

CONCLUSIONS

Although the incorporation of higher LiTFSI content significantly enhances ionic conductivity, it also results in reduced mechanical stability due to an increased plasticization of the polymer structure. Therefore, the most conductive membranes are not yet suitable for practical handling or device integration. Future work will focus on reinforcement strategies, such as polymer blending or the incorporation of suitable binders/plasticizers (*e.g.*, glycerol or sorbitol), in order to improve film robustness while maintaining efficient ionic transport.

The DSC analyses for the polymer membranes exhibit a step-like anomaly around 306 and 323 K. This anomaly, which shifts towards lower temperature values as the LiTFSI salt concentration is increased, is associated with the T_g of the new electrolytes. An decrease in T_g values indicates an increase in the amorphous phase fraction.

An increase in conductivity was observed when the temperature was varied from 283 to 358 K. This increase follows an Arrhenius behavior for all samples, suggesting that the ionic conduction of this system is a thermally activated process, with activation energies ranging between 0.20 and 0.28 J.

It should also be noted that the electrochemical window narrows slightly when the LiTFSI concentration exceeds 50%.

The conductivity isotherms, as a function of the LiTFSI concentration, showed that the ionic conductivity of the electrolytes increases with increasing salt contents, reaching a maximum value of 9.79×10^{-3} S·cm^{-1} at room temperature for a concentration of 50 wt.% LiTFSI. This behavior can be attributed to the higher number of charge carriers generated by salt dissociation, enhancing ion transport through the polymer matrix. These results indicate that the rice starch-LiTFSI membranes exhibit promising ionic conductivity and electrochemical performance. However, further studies, including full-cell testing and mechanical reinforcement, are necessary to validate their practical applicability in energy storage devices.

ACKNOWLEDGEMENTS

This research was supported by the University of Tolima.

Authors' Contribution:

Miguel Ibán Delgado Rosero: Membrane synthesis, performance of Differential Scanning Calorimetry measurements, and writing of the manuscript.
Nori Magali Jurado Meneses: Performance of measurements, analysis of impedance spectroscopy, and analysis of electrical properties.
Ramiro Uribe Kaffure: Measurements and analysis of cyclic voltammetry and writing and revision of the manuscript.

REFERENCES

Arrieta, A. A., Calabokis, O. P., & Mendoza, J. M. (2023). Effect of lithium salts on the properties of cassava starch solid biopolymer electrolytes. *Polymers*, *15*(20), 4150. https://doi.org/10.3390/polym15204150

Arrieta, A. A., Calabokis, O. P., & Vanegas, C. (2024). Influence of lithium triflate salt concentration on structural, thermal, electrochemical, and ionic conductivity properties of cassava starch solid biopolymer electrolytes. *International Journal of Molecular Sciences*, *25*(15), 8450. https://doi.org/10.3390/ijms25158450

Arya, A., & Sharma, A. L. (2019). Tailoring of the structural, morphological, electrochemical, and dielectric properties of solid polymer electrolyte. *Ionics*, *25*(4), 1617-1632. https://doi.org/10.1007/s11581-019-02916-7

Aziz, S. B., Abdulwahid, R. T., Mohammed, P. A., Rashid, S. O., Abdalrahman, A. A., Karim, W. O., Al-Asbahi, B. A., Ahmed, A. A. A., & Kadir, M. F. Z. (2024). Steps towards the ideal CV and GCD results with biodegradable polymer electrolytes: Plasticized MC based green electrolyte for EDLC application. *Journal of Energy Storage*, *76*, 109730. https://doi.org/10.1016/j.est.2023.109730

Bandara, T. M. W. J., Senavirathna, S. L. N., Wickramasinghe, H. M. N., Vignarooban, K., De Silva, L. A., Dissanayake, M. A. K. L., Albinsson, I., & Mellander, B. E. (2020). Binary counter ion effects and dielectric behavior of iodide ion conducting gel-polymer electrolytes for high-efficiency quasi-solid-state solar cells. *Physical Chemistry Chemical Physics : PCCP*, *22*(22), 12532-12543. https://doi.org/10.1039/d0cp01547d

Bósquez-Cáceres, M. F., Hidalgo-Bonilla, S., Córdova, V. M., Michell, R. M., & Tafur, J. P. (2021). Nanocomposite polymer electrolytes for zinc and magnesium batteries: From synthetic to biopolymers. *Polymers*, *13*(24), 4284. https://doi.org/10.3390/polym13244284

Bradford, G., Lopez, J., Ruza, J., Stolberg, M. A., Osterude, R., Johnson, J. A., Gomez-Bombarelli, R., & Shao-Horn, Y. (2022). Chemistry-informed machine learning for polymer electrolyte discovery. *ACS Central Science*, *9*, 206-216. https://doi.org/10.1021/acscentsci.2c01123

Chatterjee, B., Kulshrestha, N., & Gupta, P. N. (2016). Nano composite solid polymer electrolytes based on biodegradable polymers starch and poly vinyl alcohol. *Measurement: Journal of the International Measurement Confederation*, *82*, 490-499. https://doi.org/10.1016/j.measurement.2016.01.022

Dennis, J. O., Shukur, M. F., Aldaghri, O. A., Ibnaouf, K. H., Adam, A. A., Usman, F., Hassan, Y. M., Alsadig, A., Danbature, W. L., & Abdulkadir, B. A. (2023). A review of current trends on polyvinyl alcohol (PVA)-based solid polymer electrolytes. *Molecules, 28*(4), 1781. https://doi.org/10.3390/molecules28041781

Gucci, F., Grasso, M., Shaw, C., Leighton, G., Marchante Rodriguez, V., & Brighton, J. (2023). PEO-based polymer blend electrolyte for composite structural battery. *Polymer-Plastics Technology and Materials, 62*(8), 1019-1028. https://doi.org/10.1080/25740881.2023.2180391

Hina, M., Bashir, S., Kamran, K., Almomani, F., Ahmad, J., Kamarulazam, F., Ramesh, S., Ramesh, K., & Mujtaba, M. A. (2024). Energy storage devices based on flexible and self-healable hydrogel electrolytes: Recent advances and future prospects. In *Journal of Energy Storage, 85*, 110961. https://doi.org/10.1016/j.est.2024.110961

Jagan, M., & Vijayachamundeeswari, S. P. (2023). A comprehensive investigation of Lithium-based polymer electrolytes. *Journal of Polymer Research*, *30*(6), 250. https://doi.org/10.1007/s10965-023-03623-8

Jansi, R., Shenbagavalli, S., Revathy, M. S., Deepalakshmi, S., Indumathi, P., & Mohammed, M. K. A. (2023). Structural and ionic transport in biopolymer electrolyte-based PVA: NaAlg with NH_4Cl for electrochemical applications. *Journal of Materials Science: Materials in Electronics*, *34*(11), 1-15. https://doi.org/10.1007/s10854-023-10302-3

Jurado, N. M., Delgado, I., & Vargas, R. A. (2013). Ionic conductivity of $(PEO)_{10}(CF_3COONa)$-X % Al_2O_3 composites. *Universitas Scientiarum*, *18*(2), 173-180. https://doi.org/10.11144/Javeriana.SC18-2.cinc

Kalhoff, J., Bresser, D., Bolloli, M., Alloin, F., Sanchez, J. Y., & Passerini, S. (2014). Enabling LiTFSI-based electrolytes for safer lithium-ion batteries by Using linear fluorinated carbonates as (Co)solvent. *ChemSusChem*, *7*(10), 2939-2946. https://doi.org/10.1002/cssc.201402502

Kumar, D., & Hashmi, S. A. (2010). Ion transport and ion-filler-polymer interaction in poly(methyl methacrylate)-based, sodium ion conducting, gel polymer electrolytes dispersed with silica nanoparticles. *Journal of Power Sources*, *195*(15), 5101-5108. https://doi.org/10.1016/j.jpowsour.2010.02.026

Mali, S., Grossman, M. V., & Yamashiota, F. (2010). Starch films: Production, properties and potential of utilization. Semina: Ciencias Agrarias, 31(1), 137-156.

Mart, E. G. (2017). *Preparación de nuevos nanocomposites multifuncionales de matriz epoxi basados en el empleo de materiales grafénicos*. Universidad de La Rioja, Servicio de Publicaciones.

Méry, A., Rousselot, S., Lepage, D., & Dollé, M. (2021). A critical review for an accurate electrochemical stability window measurement of solid polymer and composite electrolytes. *Materials, 14*(14), 3840. https://doi.org/10.3390/ma14143840

Mishra, K., Pundir, S. S., & Rai, D. K. (2017). Effect of polysorbate plasticizer on the structural and ion conduction properties of PEO–NH_4PF_6 solid polymer electrolyte. *Ionics*, *23*(1), 105-112. https://doi.org/10.1007/s11581-016-1790-2

Ong, A. C. W., Shamsuri, N. A., Zaine, & S. N. A., Panuh, D., & Shukur, M. F. (n.d.). *Nanocomposite polymer electrolytes comprising starch-lithium acetate and titania for all-solid-state supercapacitor*. https://doi.org/10.1007/s11581-020-03856-3/Published

Rai, K. J., Saini, D. S., Shahi, P., Chaurasia, S., Yadav, D., Srivastava, N., Mishra, R., & Kumar, M. (2025). The effect of ceramic nanofillers on conductivity and ion-transport behavior in potato starch-based solid bio-polymer electrolyte for advanced energy storage devices. *Ionics*, *31*(2), 1623-1636. https://doi.org/10.1007/s11581-024-06039-6

Rasali, N. M. J., Nagao, Y., & Samsudin, A. S. (2019). Enhancement on amorphous phase in solid biopolymer electrolyte based alginate doped NH_4NO_3. *Ionics*, *25*(2), 641-654. https://doi.org/10.1007/s11581-018-2667-3

Sharma, P., & Banerjee, D. (2025). Biopolymers as solid polymer electrolytes: advances, challenges, and future prospects. *Prabha Materials Science Letters*, *4*(2), 128-147. https://doi.org/10.33889/pmsl.2025.4.2.012

Singh, C. P., Shukla, P. K., & Agrawal, S. L. (2020). Ion transport studies in PVA:NH_4CH_3COO gel polymer electrolytes. *High Performance Polymers*, *32*(2), 208-219. https://doi.org/10.1177/0954008319898242

Singh, P., Bharati, D. C., Kumar, H., & Saroj, A. L. (2019). Ion transport mechanism and dielectric relaxation behavior of PVA-imidazolium ionic liquid-based polymer electrolytes. *Physica Scripta*, *94*(10), 105801. https://doi.org/10.1088/1402-4896/ab19d9

Tang, X., & Alavi, S. (2011). Recent advances in starch, polyvinyl alcohol based polymer blends, nanocomposites and their biodegradability. *Carbohydrate Polymers, 85*(1), 7-16. https://doi.org/10.1016/j.carbpol.2011.01.030

Whba, R. A. G., TianKhoon, L., Su'ait, M. S., Rahman, M. Y. A., & Ahmad, A. (2020). Influence of binary lithium salts on 49% poly(methyl methacrylate) grafted natural rubber based solid polymer electrolytes. *Arabian Journal of Chemistry*, *13*(1), 3351-3361. https://doi.org/10.1016/j.arabjc.2018.11.009

Yadav, M., Kumar, M., & Srivastava, N. (2023). High-conducting, economical, and flexible polymer-in-salt electrolytes (PISEs) suitable for energy devices: a reality due to glutaraldehyde crosslinked starch as host. *Journal of Solid State Electrochemistry*, *27*(5), 1213-1226. https://doi.org/10.1007/s10008-023-05421-0

Yang, W., Yang, W., Zeng, J., Chen, Y., Huang, Y., Liu, J., Gan, J., Li, T., Zhang, H., Zhong, L., & Peng, X. (2024). Biopolymer-based gel electrolytes for electrochemical energy Storage: Advances and prospects. *Progress in Materials Science, 144*, 101264. https://doi.org/10.1016/j.pmatsci.2024.101264

Yong, J., Chen, Y. C., Aziz, S. B., Khandaker, M. U., & Woo, H. J. (2025). Correlated barrier hopping dynamics of Na+ ions in poly(vinyl alcohol) biopolymer-based solid polymer electrolytes: Electrical and structural analysis. *Electrochimica Acta*, *513*, 145610. https://doi.org/10.1016/j.electacta.2024.145610

Yue, J., Zhang, S., Wang, X., Fu, J., Xu, Y., Weng, S., Zhu, Y., Zhao, C., Zheng, M., Wang, Y., Zhu, X., Wu, H., Wang, G., Xia, Y., Cao, M., Jing, Q., Wang, X., Xia, W., Liang, J., … Li, X. (2025). Universal superionic conduction via solid dissociation of salts in van der Waals materials. *Nature Energy*, *10*(10), 1237-1250. https://doi.org/10.1038/s41560-026665-01853-2

Zougar, S., Morakchi, K., Zazoua, A., Saad, S., Kherrat, R., & Jaffrezic-Renault, N. (2008). Characterization of ammonium ion - Sensitive membranes in solution with electrochemical impedance spectroscopy. *Materials Science and Engineering C*, *28*(5-6), 1020-1023. https://doi.org/10.1016/j.msec.2007.10.081